Published in final edited form as:
Curr Opin Biotechnol. 2009 February ; 20(1): 90–99. doi:10.1016/j.copbio.2009.02.003.

Plasma-mediated ablation: An optical tool for submicrometer surgery on neuronal and vascular systems

Philbert S. Tsai[1], **Pablo Blinder**[1], **Benjamin J. Migliori**[1], **Joseph Neev**[2], **Yishi Jin**[3,4], **Jeffrey A. Squier**[5], and **David Kleinfeld**[1,4,¶]

[1]Department of Physics, University of California at San Diego, 9500 Gilman Drive 0374, La Jolla, CA 92093-0374

[2]FemtoSec Tech, Inc., 27068 South La Paz Road, Aliso Viejo, CA 92656

[3]Division of Biological Sciences, Howard Hughes Medical Institute, University of California at San Diego, 9500 Gilman Drive 0368, La Jolla, CA 92093-0368

[4]Graduate Program in Neurosciences, University of California at San Diego, 9500 Gilman Drive 0662, La Jolla, CA 92093-0662

[5]Department of Physics, Colorado School of Mines, 1523 Illinois Street, Golden, CO 80401

Abstract

Plasma-mediated ablation makes use of high energy laser pulses to ionize molecules within the first few femtoseconds of the pulse. This process leads to a submicrometer-sized bubble of plasma that can ablate tissue with negligible heat transfer and collateral damage to neighboring tissue. We review the physics of plasma-mediated ablation and its use as a tool to generate targeted insults at the subcellular level to neurons and blood vessels deep within nervous tissue. Illustrative examples from axon regeneration and microvascular research illustrate the utility of this tool. We further discuss the use of ablation as an integral part of automated histology.

The classic application of light microscopy to studies in physiology is observational; the illumination is too weak to affect the preparation. Yet the focused illumination in light microscopy can be strong enough to influence the chemical and physical structure of the sample and thus constitutes a means to manipulate living preparations. At the level of molecular studies, optical tweezers allow the application of forces and torques to individual molecules attached to dielectric microspheres [1,2]. At the level of subcellular organelles, photo-switching of fluorescent labels can toggle molecules between active and inactive states [3,4], while photo-activation of ions and small molecules provide a means to alter the chemical milieu within diffraction-limited volumes [5]. At the level of cells, photo-switching of bound ligands can lead to agonist binding [6], while light-activated membrane channels and pumps provide a means to change the electrical potential across cell membranes [7]. Lastly, at the level of tissue, plasma-mediated ablation provides a means to

---

[¶]Correspondence: David Kleinfeld, Department of Physics, University of California at San Diego, 9500 Gilman Drive 0374, La Jolla, CA 92093-0374, email: dk@physics.ucsd.edu.

Integrated studies of biology: Multiplexed imaging assays from molecules to man. Editors: Kevin W. Eliceiri and Christopher H. Contag

cut diffraction-limited volumes of tissue, with minimal heating, and thus to transect cells and their processes within a larger volume [8,9]. This last application is the subject of this review.

Principles and practice of plasma-mediated ablation

Pulsed laser systems easily achieve the high instantaneous peak powers necessary to induce nonlinear absorption, while maintaining sufficiently low average powers to avoid linear heating of the sample. This enables nonlinear imaging of biological structure and function [10], including two-photon laser scanning microscopy [11–13], second [14–16] and third harmonic [17–22] imaging, and coherent anti-stokes Raman spectroscopy [23,24]. The critical issue, especially for *in vivo* imaging, is that the nonlinear absorption allows excitation to occur only in the focus volume so that all excited molecules are a potential source of signal. Thus optical sectioning is performed solely by the excitation beam. Fluorescently labeled cells deep below the surface of brain tissue, as much as 1000 μm under optimal conditions, may be imaged [25–27].

Plasma-mediated ablation with pulsed laser excitation builds on the concept of local excitation through nonlinear absorption, yet uses energy levels that are high enough to tear molecules apart that rather than just drive electronic transitions that lead to fluorescent relaxation [8]. Energy fluence, defined as the energy per unit area in the pulse, is a natural metric to describe the extent of material damage produced by a short laser pulse focused to a spot. As an example, consider a 100-nJ, 100-fs pulse that is focused to an 1-μm^2 area; this yields a fluence of 1 J/cm^2 or equivalently, an intensity of 10^{13} W/cm^2 and an electric field of ~ 10^8 V/cm (Fig. 1). This field is within an order of magnitude of the ~10^9 V/cm electric field that binds valence electrons and thus is sufficiently strong to ionize any molecules at the focus. This can lead to the formation of a bubble of plasma at the focus.

The growth of the plasma occurs as a two-step process. In the first step, bound electrons are freed from their molecular orbitals by interaction with the electric field of the laser pulse, either by a process of multiphoton absorption or Zener electron tunneling ionization [28]. In the second step, the free electrons seed an impact ionization cascade that involves acceleration of the electrons by inverse-Bremsstrahlung absorption, in which an electron absorbs photons while colliding with molecules. After several absorption events, the free electrons achieve sufficiently high kinetic energy to ionize another molecule by impact ionization. This cascade, along with the continued generation of photoelectrons, leads to the exponential growth of a micrometer-sized plasma bubble. As the electron density grows, the plasma eventually becomes sufficiently conductive to limit the penetration of the incident light to a skin depth of only tens of nanometers. This restricted penetration depth provides axial localization that is far less than the confocal length, or focal depth, of the incident light.

The termination of the laser pulse is followed by recombination of the free electrons with the positively ionized molecules at the focus. This occurs on the picosecond time scale of electron collisions at typical electron densities and leads to a transfer of energy from the electrons to the material on a timescale that is short compared to the ~ 100 ps acoustic relaxation time in the material. The result is a dramatic pressure increase within the excitation volume that can produce a rupture of the material and form a cavitation bubble. The bubble constitutes the region of ablation. The expansion of the cavitation bubble is associated with an acoustic shockwave that also propagates into the surrounding tissue (Fig. 2a) and has the potentially deleterious effect of spreading damage into the sample.

Necessity of femtosecond pulses

The key aspect of plasma-mediated ablation is the generation of the initial free electrons that seed the inverse-Bremsstrahlung absorption. For near infrared light, the necessary intensity for this process is ~ 10^{11} W/cm^2 [28]. For nanosecond pulses, this is achieved with a 1-μJ, 1-ns pulse focused to a 1-μm^2 area, which corresponds to a fluence of 100 J/cm^2. In contrast, hundred-femtosecond pulses are too short-lived to achieve critical density from the cascade of a single, or few, seed electrons. Thus, for hundred-femtosecond pulses, a higher intensity irradiance, *i.e.*, ~10^{13} W/cm^2 [29], is necessary to achieve plasma-mediated ablation. This can be achieved with a 10-nJ, 100-fs pulse, focused to a 1-μm^2 area, corresponding to a fluence of 1 J/cm^2 (Fig. 1). In this case the ~10^{11} W/cm^2 intensity for seed generation is exceeded over the duration of the ultrashort pulse, during which time both seed generation and avalanche cascade act concurrently to reach the critical electron density. Notably, the total pulse energy for the hundred-femtosecond case is a factor of 100 less than for nanosecond pulses, which substantially reduces collateral damage from heating, bubble expansion, and shockwave release. For this reason, ablation of fine structures is best performed with hundred-femtosecond pulses and fluences close to the threshold of approximately 1 J/cm^2.

Light sources for plasma-mediated optical ablation

The underlying architecture of all amplified femtosecond systems follows a plan that is essentially independent of the gain medium [30,31]. First, the pulse train from a hundred-femtosecond oscillator is subsampled and sent to an optical stretcher, which expands the pulse width from hundreds of femtoseconds to hundreds of picoseconds. Second, the stretched pulses pass through a gain stage, which increases their energy from nanojoules to upwards of a millijoule. Finally, an optical compressor restores the pulse width to the original hundred-femtosecond width [32]. Heat dissipation by the gain stage suggests the need to maintain an average power level of one to three Watts throughout the system. Optical amplifiers operate at much lower repetition rates, typically one to several hundreds of kilohertz, than the hundred megahertz of oscillators. For an average power of one to three Watts, the corresponding pulse energy is 1 mJ per pulse. For amplified, compressed pulse durations on the order of 100 fs, these pulse energies and repetition rates are sufficient to enable rapid ablation of tissue near the surface or to allow high-precision ablation deep within scattering tissues.

Ti:sapphire-based femtosecond oscillator/amplifiers are presently the dominant choice of laser system for concurrent imaging and ablation, with most amplifiers tuned near the peak of the fluorescent spectrum of Ti:sapphire at λ_{center} = 800 nm [33]. Ytterbium-based systems have desirable average power characteristics for an amplifier [34,35], although they feature slightly longer pulse widths, *i.e.*, ~200 fs or greater. Further, because Ytterbium-based systems operate at λ_{center} = 1030 to 1070 nm, where dispersion is low, they require little, if any, dispersion compensation. From a more pragmatic point of view, Ytterbium sources can be pumped with inexpensive, long-lasting semiconductor diode lasers, which make them very cost-effective systems to use and maintain. The design of amplified laser systems is an ongoing, competitive process [36], with fiber-based lasers as the latest emerging design [37].

Importance of beam profile

A key parameter for ablation is the spatial profile of the beam, as hot spots on the focused beam profile can result in a striated ablation zone. It is desirable to maintain a flat spectral phase, a flat spatial phase front, and smooth spatial and spectral amplitudes to achieve the best possible ablation conditions. Interferometric methods exist for concurrently measuring the spatial and spectral characteristics of an ultrashort pulse [38]. In essence, the pulse from the microscope is interfered with a reference pulse using a Michelson interferometer, where

the microscope is one arm of the interferometer. The output of the interferometer is recorded through an imaging spectrometer so that spatial information is on one axis and spectral information is along the second axis of the resultant interferogram. This allows the spectral and spatial phase and amplitude characteristics of the beam to be extracted simultaneously. For example, Amir *et al*. [38] directly measured the increase in duration of a 50-fs laser pulse that was focused by a 1.25 NA, 100-times magnification oil immersion objective. The increase in duration at the focus resulted from spherical and chromatic aberrations; the former aberration leads to a larger focal spot size and will degrade the optical performance of an ablation system.

Realization

Plasma-mediated ablation is best used in coordination with an imaging system. For subsurface ablation, this requires the integration of an amplified hundred-femtosecond source with a two-photon laser scanning microscope. The two beams may be combined with a dichroic beam splitter if they are at different wavelengths. However, since Ti:sapphire oscillators are usually used for both imaging and ablation beams, it is convenient to combine them with a polarizing beam splitter. A specific realization has been detailed [39–41], together with software to drive the composite system [42].

Examples from nonliving samples

The sharp threshold and reproducibility of ablation with hundred-femtosecond pulses has been exploited to produce reliable sub-diffraction limited features in a broad range of materials [28,43,44]. For example, Joglekar *et al*. [28]; have produced holes with diameters of ~100 nm in glass using a λ_{center} = 1.053 μm excitation wavelength and pulse widths on the order of 800 fs (Figs. 2b and 2c). Conversely, for large-scale ablation, the low energy fluence threshold for hundred-femtosecond pulses results in minimal mechanical and thermal collateral damage compared to longer pulses. While biological samples pose challenges that may mitigate such fine control of ablation, the results for glass provide a proof of principle for what may be achieved.

Applications of plasma-mediated ablation to neurobiology

Plasma-mediated ablation has been applied to many preparations in biology [9], from cutting subcellular organelles in cultured cells [45–47] and processes in multicellular organisms [48–52] to ablating bone, dentine and enamel [53], cornea [54–56], epithelia [57], neuronal [39,58–60] and vascular [40] tissue. Here we focus on applications in neurobiology, where pulse energies and focus points are typically chosen to remove larger volumes of material than is the case for minimal ablation of a glass surface. This typically results in ~ 1 μm cuts (Figs. 2d and 2e).

Axon cutting and regeneration

The roundworm *Caenorhabditis elegans* is composed of 959 somatic cells, 302 of which are neurons. Axons in *C. elegans* grow either directly over basement membranes or form bundles of up to 120 processes. The worm is optically transparent, and transgenic expression of fluorescent proteins in neurons allows direct visualization of individual nerves in living animals. Recent work exploits these optical properties to perform plasma-mediated ablation of single axons in live animals [48–52]; the example in Figure 3 shows ablation and regrowth of mechanosensory neurons.

The use of plasma-mediated ablation provides a unique means to study regrowth of the damaged axon as well as recovery of physiological behavior. This led to the realization that several types of neurons can regenerate rapidly following a single cut in the axon. The rate

and precision of regenerative growth by the injured axons exhibits cell type, process type and developmental stage specificity. For example, mechanosensory axon regrowth varies depending on whether the axon is cut proximal or distal to a collateral synaptic branch [49]. The intrinsic growth ability of severed axons requires known cytoskeletal regulators, such as Lamellipodin and Enabled [50]. The combination of a large set of genetic mutants and RNA interference is facilitating investigation of the genetic factors influencing axon regeneration in a semi-permissive environment. In addition, the precision of plasma-mediated ablation has helped to determine the roles of specific cell processes in behaviors such as thermosensation [61] and egg-laying [62].

The development of microfluidic chambers to immobilize animals in the absence of anesthetic gives promise to overcome the technical hurdles of time-lapse imaging of regenerating axons and repair [61,63,64]. By combining microfluidic devices with automated imaging and plasma-mediated ablation, it may be possible to perform high-throughput studies of neuronal damage responses [63].

in situ keratomileusis

In traditional laser *in situ* keratomileusis (LASIK), a microkeratome is used to mechanically cut a corneal flap that is 100 to 200 μm in thickness. An eximer laser is then used to ablate the stromal bed of the cornea, after which the corneal flap is replaced. In a recent incarnation of LASIK, plasma-mediated ablation is used to make a subsurface cut in the cornea to generate the flap, obviating the need for a microkeratome [65]. As in the traditional case, an eximer laser is used to ablate the stromal bed of the cornea. The use of plasma-mediated ablation has the potential advantage of making a thinner and more uniform corneal flap compared with the use of a microkeratome [66]. Beyond this, there are currently no clear differences in the long-term surgical outcome of the two methods [67,68].

Vascular occlusion and models of stroke

Until recently, manipulation of cortical blood flow in animal models of stroke has been limited to large-scale occlusions that stop or reduce flow to a large fraction of the cortical vasculature [69]. Recently, a technique was developed that utilizes hundred-femtosecond laser pulses to disrupt the flow in a single cortical microvessel [40,70]. A cranial window is implanted in an anesthetized rat to gain optical access to neocortex, and blood plasma is fluorescently labeled by intravenous injection of fluorescein-isothiocyanate-dextran so that blood cells appear as dark objects on a bright background [71–73]. The motion of red blood cells (RBCs) as well as the diameter of the vessel are visualized through water-immersion objectives using two photon microscopy.

By focusing low-to-moderate energy laser pulses, *i.e.*, 0.1 to 1 μJ, into the lumen of a microvessel, three models of vascular disruption could be generated (Fig. 4). The application of a single ~ 1 μJ pulse could produce a complete rupture of the individual vessel, while flow is left intact in surrounding vessels. This hemorrhagic rupture released both blood plasma and RBCs into the surrounding tissue. In contrast, extravasation of blood plasma into the extracellular space, but no interruption in the flow of RBCs, is induced when the pulse energy is reduced to between 0.1 and 0.5 μJ. Finally, continued ablation of the targeted vessel with additional pulse of the same energy led to the formation of a clot and cessation of blood flow within the targeted vessel.

This technique provides a singular means to target occlusion to subsurface vessels. Studies to date have shown that blockage of a single microvessel leads to disruption of flow at the nearest and next-nearest downstream vessels, but that the disturbance is ameliorated for more distant vessels presumably by the presence of loops within the vascular network [40].

The ability to monitor flow before and after an occlusion suggests that this technique may be applicable to the study of interventional therapies for microstrokes.

All-optical histology

The activity of neuronal cells relies critically on blood flow in the brain to supply them with oxygen and nutrients and to remove waste and heat. Changes in the distribution of blood, as occurs both physiologically during heightened mental activity and pathologically during disease states, impact the function and survivability of the surrounding tissue. To quantify the distribution of cortical blood flow, as well as its dynamic response to changes in energetic needs, an angiotome, i.e., a complete fully-connected three-dimensional map of brain vasculature, is required.

As a means to complete the angiotome, all-optical histology [39] utilizes two-photon laser scanning microscopy coupled with plasma-mediated ablation to image vascular structures throughout millimeter-scale blocks of histological cortical tissue (Fig. 5a). Plasma-mediated ablation with moderate pulse energies, *i.e.*, ~ 1 μJ, is used to remove ~ 1 pL of tissue per pulse from the previously-imaged surface, thereby exposing underlying tissue for the next round of two-photon imaging. Overlapping image stacks are taken that range in depth from 50 to 150 μm, depending on the optical quality of the tissue, and nominally two-thirds of the previously imaged tissue is removed at each round of ablation.

After the entire tissue block has been processed in this manner, a three-dimensional montage is made from the individual image blocks; this is illustrated in Figure 5b for a cubic millimeter of fluorescently-labeled vasculature in mouse cortex. Algorithms for the automatic vectorization of these vascular structures along with segmentation and classification of surrounding neuronal tissue are currently being developed [74,75]. Lastly, all-optical histology should be appropriate for the reconstruction of labeled neurons at the level of tracing axonal projections and dendritic arborization, albeit not synaptic contacts.

Thermal tissue damage at subcritical levels of fluence

Intermediate levels of fluence can produce seed electrons but are insufficient to drive the cascade of ionization that leads to formation of a high-density plasma followed by material rupture and cavitation. Nonetheless, the production of low-density plasma and the pulse-to-pulse accumulation of heat can act to locally modify the tissue by chemical and thermal means. This procedure has been used to disrupt cell membranes for transient cell transfection [47], as well as induce damage to dendritic processes [76] and vascular walls [77]. The nonlinear absorption of infrared light by hemoglobin contributes to the heating process at fluences greater than 0.05 J/cm^2 [78].

Emerging application to neuronal cell ablation

The use of plasma-mediated laser ablation to perturb a biological system holds two major advantages over traditional techniques, such as electrical or pharmacological ablation of large tissue regions. The first is the high degree of localization of damage. This allows for selective ablation of subcellular structures, as illustrated by the axon cutting [48] (Fig. 3) discussed above, as well as by work on the ablation of mitochondria [79,80]. The second advantage is the ability to target many more individual cells for manipulation than would be feasible by mechanical methods, including those that involve a micropipet to deliver pharmaceuticals.

Network phenomena and the convergence of multiple inputs onto a single cell, cortical column, or vascular unit all play important roles in neurophysiology. The ability to progressively remove selected inputs to a system while simultaneously monitoring the

resultant change in dynamics *in vivo* may help elucidate emergent properties of nervous systems. The use of femtosecond plasma-mediated ablation to remove multiple neurons of a specific neuronal subclass, as identified by cell-specific endogenous fluorescence in transgenic mice, is being actively pursued. Pilot studies have demonstrated the ability to ablate a cell while maintaining normal electrophysiological responses in neighboring cells (Fig. 6). Techniques that use genetic manipulation and chemical induction to inactivate specific neuronal subclasses will be more selective than plasma-mediated ablation and have the further potential advantage of reversibility [81]. However, ablation has an advantage as a rapid method that does not rely on the fabrication of new animals.

Conclusions

The deterministic, self-limiting and fine-resolution features of plasma-mediated ablation with hundred-femtosecond pulses make it attractive as a precise neurosurgical tool. Ongoing *in vivo* applications include the targeted ablation of cellular components, including axons, somata, and microvessels, as a tool to study the response of brain cells to direct perturbations. Additional applications include automated, block-face imaging of fixed tissue and the possible extension to automated surgery of bone, chitin, and corneas of living preparations.

Acknowledgments

We thank our collaborators Bassam Atallah and Massimo Scanziani for their assistance with obtaining the data in figure 6, Adrienne L. Fairhall for comments on the manuscript, and the HHMI (YJ), the ISF Bikura program (PB), the NIH (EB003832 to DK and JAS, MH085499 and RR021907 to DK, and NS35546 to YJ), and the NSF (DBI 0455027 to DK) for generous funding.

References

1. Block SM. Making light work with optical tweezers. Nature. 1992; 360:493–496. [PubMed: 1448176]
2. Judkewitz B, Roth A, Häusser M. Dendritic enlightenment: Using patterned two-photon uncaging to reveal the secrets of the brain's smallest dendrites. Neuron. 2006; 50:180–183. [PubMed: 16630828]
3. Ando R, Hama H, Yamamoto-Hino M, Mizuno H, Miyawaki A. An optical marker based on the UV-induced green-to-red photoconversion of a fluorescent protein. Proceedings of the National Academy of Sciences USA. 2002; 99:12651–12656.
4. Habuchi S, Ando R, Dedecker P, Verheijen W, Mizuno H, Miyawaki A, Hofkens J. Reversible single-molecule photoswitching in the GFP-like fluorescent protein Dronpa. Proceedings of the National Academy of Sciences USA. 2005; 102:9511–9516.
5. Denk W, Delaney KR, Kleinfeld D, Strowbridge B, Tank DW, Yuste R. Anatomical and functional imaging of neurons and circuits using two photon laser scanning microscopy. Journal of Neuroscience Methods. 1994; 54:151–162. [PubMed: 7869748]
6. Baghart M, Borges K, Isacoff EY, Kramer RH. Light-activated ion channels for remote control of neuronal firing. Nature Neuroscience. 2004; 7:1381–1386.
7. Zhang F, Wang L-P, Brauner M, Liewald JF, Ka K, Watzke N, Wood PG, Bamberg E, Nagel G, Gottschalk A, et al. Multimodal fast optical interrogation of neural circuitry. Nature. 2007; 446:633–641. [PubMed: 17410168]
8. Vogel A, Noack J, Huttman G, Paltauf G. Mechanisms of femtosecond laser nanosurgery of cells and tissues. Applied Physics B-Lasers and Optics. 2005; 81:1015–1047.
9. Tsai PS, Friedman B, Squier JA, Kleinfeld D. Ultrashort pulsed laser light: A cool tool for ultraprecise cutting of tissue and cells. Optics and Photonic News. 2004; 14:24–29.
10. Zipfel WR, Williams RM, Webb WW. Nonlinear magic: Multiphoton microscopy in the biosciences. Nature Biotechnology. 2003; 21:1369–1377.

11. Denk W, Strickler JH, Webb WW. Two-photon laser scanning fluorescence microscopy. Science. 1990; 248:73–76. [PubMed: 2321027]
12. Denk W, Svoboda K. Photon upmanship: Why multiphoton imaging is more than a gimmick. Neuron. 1997; 18:351–357. [PubMed: 9115730]
13. Svoboda K, Yasuda R. Principles of two-photon excitation microscopy and its applications to neuroscience. Neuron. 2006; 50:823–839. [PubMed: 16772166]
14. Moreaux L, Sandre O, Blanchard-Desce M, Mertz J. Membrane imaging by simultaneous second-harmonic generation and two-photon microscopy. Optics Letters. 2000; 25:320–322. [PubMed: 18059867]
15. Campagnola PJ, Clark HA, Mohler WA, Lewis A, Loew LM. Second-harmonic imaging microscopy of living cells. Journal of Biomedical Optics. 2001; 6:277–286. [PubMed: 11516317]
16. Campagnola PJ, Loew LM. Second-harmonic imaging microscopy for visualizing biomolecular arrays in cells, tissues and organisms. Nature Biotechnology. 2003; 21:1356–1360.
17. Barad Y, Eisenberg H, Horowitz M, Silberberg Y. Nonlinear scanning laser microscopy by third harmonic generation. Applied Physics Letters. 1997; 70:922–924.
18. Squier J, Muller M, Brakenhoff GJ, Wilson K. Third harmonic generation microscopy. Optics Express. 1998; 3:315–321. [PubMed: 19384376]
19. Oron D, Yelin D, Tal E, Raz S, Fachima R, Silberberg Y. Depth-resolved structural imaging by third-harmonic generation microscopy. Journal of Structural biology. 2004; 147:3–11. [PubMed: 15109600]
20. Yelin D, Oron D, Korkotian E, Segal M, Silberberg Y. Third-harmonic microscopy with a titanium-sapphire laser. Applied Physics B. 2002; 74:97–101.
21. Yelin D, Silberberg Y. Laser scanning third-harmonic microscopy in biology. Optics Express. 1999; 5:169–175. [PubMed: 19399061]
22. Clay GO, Millard AC, Schaffer CB, Aus-der-Au J, Tsai PS, Squier JA, Kleinfeld D. Spectroscopy of third harmonic generation: Evidence for resonances in model compounds and ligated hemoglobin. Journal of the Optical Society of America B. 2006; 23:932–950.
23. Zumbusch A, Holtom GR, Xie XS. Three dimensional Vibrational Imaging by coherent anti-Stokes Raman scattering. Physical Review Letters. 1999; 82:4142–4145.
24. Cheng JX, Xie XS. Coherent anti-Stokes Raman scattering microscopy: Instrumentation, theory, and applications. Journal of Physical Chemistry B. 2004; 108:827–840.
25. Helmchen F, Denk W. Deep tissue two-photon microscopy. Nature Methods. 2005; 2:932–940. [PubMed: 16299478]
26. Oheim M, Beaurepaire E, Chaigneau E, Mertz J, Charpak S. Two-photon microscopy in brain tissue: Parameters influencing the imaging depth. Journal of Neuroscience Methods. 2001; 111:29–37. [PubMed: 11574117]
27. Theer P, Denk W. On the fundamental imaging-depth limit in two-photon microscopy. Journal of the Americal Optical Society A. 2006; 23:3139–3150.
28. Joglekar AP, Liu HH, Meyhofer E, Mourou G, Hunt AJ. Optics at critical intensity: Applications to nanomorphing. Proceedings of the National Academy of Sciences USA. 2004; 101:5856–5861.
29. Stuart BC, Feit MD, Herman S, Rubenchik AM, Shore BW, Perry MD. Nanosecond-to-femtosecond laser-induced breakdown in dielectrics. Physical Review B. 1996; 53:1749–1761.
30. Maine P, Strickland D, Bado P, Pessot M, Mourou G. Generation of ultrahigh peak power pulses by chirped pulse amplification. IEEE Journal of Quantum Electronics. 1988; 24:398–403.
31. Knox WH. Femtosecond optical pulse amplification. IEEE Journal of Quantum Electronics. 1988; 24:388–397.
32. Strickland D, Mourou G. Compression of amplified chirped optical pulses. Optics Communications. 1985; 55:447–449.
33. Backus S, Durfee CG III, Murnane MM, Kapteyn HC. High power ultrafast lasers. Review of Scientific Instruments. 1998; 69:1207–1223.
34. Brunner F, Sphler GJ, Aus der Au J, Krainer L, Morier-Genoud F, Paschotta R, Lichtenstein N, Weiss S, Harder C, Lagatsky AA, et al. Diode-pumped femtosecond Yb:KGd(WO4)2 laser with 1.1-W average power. Optics Letters. 2000; 25:1119–1121. [PubMed: 18064290]

35. Honninger C, Paschotta R, Graf M, Morier-Genoud, Zhang FG, Moser M, Biswal S, Nees J, Brau A, Mourou GA, et al. UItrafast ytterbium-doped bulk lasers and laser amplifiers. Applied Physics B. 1999; 69:3–17.
36. Keller U. Recent developments in compact ultrafast lasers. Nature. 2003; 24:831–838. [PubMed: 12917697]
37. Limpert J, Roser F, Schreiber T, Tunnerman A. High-power ultrafast fiber laser systems. IEEE Journal of Quantum Electronics. 2006; 12:233–244.
38. Amir W, Planchon TA, Durfee C, Squier J, Gabolde P, Trebino R, Müller M. Simultaneous visualization of spatial and chromatic aberrations by two-dimensional Fourier transform spectral interferometry. Optics Letters. 2006; 31:2927–2929. [PubMed: 16969425]
39. Tsai PS, Friedman B, Ifarraguerri AI, Thompson BD, Lev-Ram V, Schaffer CB, Xiong Q, Tsien RY, Squier JA, Kleinfeld D. All-optical histology using ultrashort laser pulses. Neuron. 2003; 39:27–41. [PubMed: 12848930]
40. Nishimura N, Schaffer CB, Friedman B, Tsai PS, Lyden PD, Kleinfeld D. Targeted insult to individual subsurface cortical blood vessels using ultrashort laser pulses: Three models of stroke. Nature Methods. 2006; 3:99–108. [PubMed: 16432519]
41. Tsai, PS.; Kleinfeld, D. In vivo two-photon laser scanning microscopy with concurrent plasma-mediated ablation: Principles and hardware realization. In: Frostig, RD., editor. Methods for In Vivo Optical Imaging. 2nd edition.. CRC Press; 2009.
42. Nguyen, Q-T.; Dolnick, EM.; Driscoll, J.; Kleinfeld, D. MPScope 2.0: A computer system for two-photon laser scanning microscopy with concurrent plasma-mediated ablation and electrophysiology. In: Frostig, RD., editor. Methods for In Vivo Optical Imaging. 2nd edition.. CRC Press; 2009.
43. Lenzner M, Krausz F, Kruger J, Kautek W. Photoablation with sub-10 fs laser pulses. Applied Surface Science. 1999; 154–155:11–16.
44. Schaffer CB, Brodeur A, Garcia JF, Mazur E. Micromachining bulk glass by use of femtosecond laser pulses with nanojoule energy. Optics Letters. 2001; 26:93–95. [PubMed: 18033517]
45. Hoy CL, Durr NJ, Chen P, Piyawattanametha W, Ra H, Solgaard O, Ben-Yakar A. Miniaturized probe for femtosecond laser microsurgery and two-photon imaging. Optics Express. 2008; 16:9996–10005. [PubMed: 18575570]
46. Watanabe W, Arakawa N, Matsunaga S, Higashi T, Fukui K, Isobe K, Itoh K. Femtosecond laser disruption of subcellular organelles in a living cell. Optics Express. 2004; 12:4203–4213. [PubMed: 19483965]
47. Tirlapur UK, Konig K. Targeted transfection by femtosecond laser light. Nature. 2002; 418:290–291. [PubMed: 12124612]
48. Yanik MF, Cinar H, Cinar HN, Chisholm AD, Jin Y, Ben-Yakar A. Functional regeneration after laser axotomy. Nature. 2004; 432:822. [PubMed: 15602545]
49. Wu Z, Ghosh-Roy A, Yanik MF, Zhang AZ, Jin YS, Chisholm AD. Caenorhabditis elegans neuronal regeneration is influenced by life stage, ephrin signaling, and synaptic branching. Proceedings of the National Academy of Sciences USA. 2007; 104:15132–15137.
50. Gabel CV, Antonie F, Chuang CF, Samuel ADT, Chang C. Distinct cellular and molecular mechanisms mediate initial axon development and adult-stage axon regeneration in C. elegans. Development. 2008; 135:1129–1136. [PubMed: 18296652]
51. Guo SX, Bourgeois F, Chokshi T, Durr NJ, Hilliard MA, Chronis N, Ben-Yakar A. Femtosecond laser nanoaxotomy lab-on-a chip for in vivo nerve regeneration studies. Nature Methods. 2008; 5:531–533. [PubMed: 18408725]
52. Bourgeois F, Ben-Yakar A. Femtosecond laser nanoaxotomy properties and their effect on axonal recovery in C. elegans. Optics Express. 2008; 16:5963-5963–5963-5963. [PubMed: 18725955]
53. Neev J, Carrasco WA, Armstrong WB, Da Silva LB, Feit MD, Matthews DL, Perry MD, Rubenchik AM, Stuart BC. Applications of ultrashort pulse lasers for hard tissue surgery. IEEE Journal of Selected Topics in Quantum Electronics. 1996; 2:790–800.
54. Juhasz T, Loesel HL, Kurtz RM, Horvath C, Bille JF, Mourou G. Corneal refractive surgery with femtosecond lasers. IEEE Journal of Selected Topics in Quantum Electronics. 1999; 5:902–910.

55. Lubatschowski H, Maatz G, Heisterkamp A, Hetzel U, Drommer W, Welling H, Ertmer W. Application of ultrashort laser pulses for intrastromal refractive surgery. Graefe's Archives of Clinical Experimental Opthamology. 2000; 238:33–39.
56. Maatz G, Heisterkamp A, Lubatschowski H, Barcikowski S, Fallnich C, Welling H, Ertmer W. Chemical and physical side effects at application of ultrashort laser pulses for intrastromal refractive surgery. Journal of Optics A. 2000; 2:59–64.
57. Frederickson KS, White WE, Wheeland RG, Slaughter DR. Precise ablation of skin with reduced collateral damage using the femtosecond-pulsed, terawatt titanium-sapphire laser. Archives of Dermatology. 1993; 129:989–993. [PubMed: 8352623]
58. Suhm N, Gotz MH, Fischer JP, Loesel F, Schlegel W, Sturm V, Bille JF, Schroder R. Ablation of neural tissue by short-pulsed lasers-A technical report. Acta Neurochirurgica. 1996; 138:346–349. [PubMed: 8861705]
59. Oraevsky A, Da Silva L, Rubenchik A, Feit M, Glinsky M, Perry M, Mammini B, Small W, Stuart B. Plasma mediated ablation of biological tissues with nanosecond-to-femtosecond laser pulses: Relative role of linear and nonlinear absorption. IEEE Journal of Selected Topics in Quantum Electronics. 1996; 2:801–809.
60. Loesel FH, Fischer JP, Gotz MH, Horvath C, Juhasz T, Noack F, Suhm N, Bille JF. Non-thermal ablation of neural tissue with femtosecond laser pulses. Applied Physics B. 1998; 66:121–128.
61. Chung KH, Crane MM, Lu H. Automated on-chip rapid microscopy, phenotyping and sorting of C. elegans. Nature Methods. 2008; 5:637–643. [PubMed: 18568029]
62. Zhang M, Chung SH, Fang-Yen C, Craig C, Kerr RA, Suzuki H, Samuel AD, Mazur E, Schafer WR. A self-regulating feed-forward circuit controlling C. elegans egg-laying behavior. Current Biology. 2009; 14:1445–1455.
63. Rohde CB, Zeng F, Gonzalez-Rubio R, Angel M, Yanik MF. Microfluidic system for on-chip high-throughput whole-animal sorting and screening at subcellular resolution. Proceedings of the National Academy of Sciences USA. 2007; 104:13891–13895.
64. Guo SX, Bourgeois F, Chokshi T, Durr NJ, Hilliard MA, Chronis N, Ben-Yakar A. Femtosecond laser nanoaxotomy lab-on-achip for in vivo nerve regeneration studies. Nature Methods. 2008; 5:531–533. [PubMed: 18408725]
65. Mian SI, Shtein RM. Femtosecond laser-assisted corneal surgery. Current Opinion in Ophthalmology. 2007; 18:295–299. [PubMed: 17568205]
66. Binder PS, Sarayba M, Ignacio T, Juhasz T, Kurtz R. Characterization of submicrojoule femtosecond laser corneal tissue dissection. Journal of Cataract and Refractive Surgery. 2008; 34:146–152. [PubMed: 18165095]
67. Patel SV, Maguire LJ, McLaren JW, Hodge DO, Bourne WM. Femtosecond laser versus mechanical microkeratome for LASIK. Ophthalmology. 2007; 114:1482–1490. [PubMed: 17350688]
68. Chan A, Ou J, Manche EE. Comparison of the Femtosecond Laser and Mechanical Keratome for Laser In Situ Keratomileusis. Archives of Ophthalmology. 2008; 126:1484–1490. [PubMed: 19001213]
69. Chen, J.; Xu, ZC.; X-M, X.; Zhang, JH. Animal Models of Acute Neurological Injuries. Totowa: Humana Press; 2008.
70. Kleinfeld, D.; Friedman, B.; Lyden, PD.; Shih, AY. Targeted occlusion to surface and deep vessels in neocortex via linear and nonlinear optical absorption. In: Chen, J.; Xu, Z.; Xu, X-M.; Zhang, J., editors. In Animal Models of Acute Neurological Injuries. The Humana Press Inc; 2008.
71. Helmchen F, Kleinfeld D. In vivo measurements of blood flow and glial cell function with two-photon laser scanning microscopy. Methods in Enzymology. 2008; 444:231–254. [PubMed: 19007667]
72. Kleinfeld D, Mitra PP, Helmchen F, Denk W. Fluctuations and stimulus-induced changes in blood flow observed in individual capillaries in layers 2 through 4 of rat neocortex. Proceedings of the National Academy of Sciences USA. 1998; 95:15741–15746.
73. Dirnagl U, Villringer A, Einhaupl KM. *In-vivo* confocal scanning laser microscopy of the cerebral microcirculation. Journal of Microscopy. 1992; 165:147–157. [PubMed: 1552568]

74. Kaufhold J, Tsai PS, Blinder P, Kleinfeld D. MICCAI. Threshold relaxation is an effective means to connect gaps in 3D images of complex microvascular networks. Third Workshop on Microscopic Image Analysis with Applications in Biology. 2008

75. Cassot F, Lauwers F, Fouard C, Prohaska S, Lauwers-Cances V. A novel three-dimensional computer-assisted method for a quantitative study of microvascular networks of the human cerebral cortex. Microcirculation. 2006; 13:1–18. [PubMed: 16393942]

76. Sacconi L, O'Connor RP, Jasaitis A, Masi A, Buffelli M, Pavone FS. In vivo multiphoton nanosurgery of cortical neurons. Journal of Biomedical Optics. 2007; 12–050502:1–3.

77. Nimmerjahn A, Kirchhoff F, Helmchen F. Resting microglial cells are highly dynamic surveillants of brain parenchyma in vivo. Science. 2005; 308:1314–1318. [PubMed: 15831717]

78. Clay GO, Schaffer CB, Kleinfeld D. Large two-photon absorptivity of hemoglobin in the infrared range of 780–880 nm. Journal of Chemical Physics. 2007; 126 025102.

79. Shen N, Datta D, Schaffer CB, LeDuc P, Ingber DE, Mazur E. Ablation of cytoskeletal filaments and mitochondria in live cells using a femtosecond laser nanoscissor. Mechanical and Chemical Biosystems. 2005; 2:17–25.

80. Heisterkamp A, Maxwell IZ, Mazur E, Underwood JM, Nickerson JA, Kumar S, Ingber DE. Pulse energy dependence of subcellular dissection by femtosecond laser pulses. Optics Express. 2005; 13:3690–3696. [PubMed: 16035172]

81. Tervo D, Karpova AY. Rapidly inducible, genetically targeted inactivation of neural and synaptic activity in vivo. Current Opinion in Neurobiology. 2007; 17:581–586. [PubMed: 18054219]

82. Schaffer CB, Nishimura N, Glezer EN, Kim AMT, Mazur E. Dynamics of femtosecond laser-induced breakdown in water from femtoseconds to microseconds. Optics Express. 2002; 10:196–203. [PubMed: 19424350]

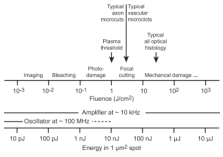

Figure 1. Scales in plasma-assisted optical ablation

A Ti:Sapphire oscillator produces a roughly 100-MHz train of 1 nJ, 100-fs pulses, to achieve a peak power of 0.1 MW at an average power of 1 W. In contrast, a current state-of-the-art amplified Ti:Sapphire system, may produce a roughly 10 kHz train of 100 μJ 100-fs pulses, to achieve a peak power of 1,000 MW at the same average power of 1 W.

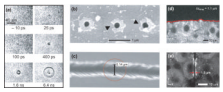

Figure 2. Phenomenology of plasma-mediated ablation

(a) Visualization of the time evolution the plasma bubble and acoustic pressure wave induced by an ~ 100 femtosecond ablation of water with a 1-mJ pulse. The visualization was effected with delayed pulses that were frequency doubled, expanded, and collimated to form an illumination beam. Adapted from Schaffer *et al*. [82]. **(b)** Scanning electron micrograph of submicrometer damage in glass that was produced by femtosecond ablation with a high numerical aperture objective near threshold pulse at the surface of the substrate. Arrows depict smooth surfaces that underlie debris that is deposited around the central crater. Adapted from Joglekar *et al*. [28]. **(c)** Scanning electron micrograph of a groove machined at a glass-water interface using a sequence of femtosecond pulses spaced 50 nm apart. The red circle indicates the e^{-2} spot size of the Gaussian laser beam. Adapted from Joglekar *et al*. [28]. **(d)** A line cut in fixed cerebellar tissue, derived from a transgenic mouse in which the Purkinje neurons are endogenously labeled with cyan fluorescent protein, with an intermediate numerical aperture (0.3 NA) objective. The bean was focused just below the tissue and thus results is a deep but wide curt; the image corresponds to maximal projections through a depth of 3 μm. Adapted from Tsai *et al*. [39]. **(d)** Detail of the ablated surface for fixed cortex from mouse cut with hundred-femtosecond pulsed laser light. The laser was focused onto the cut face with an intermediate numerical aperture objective (0.5 NA) and single passes were made to optically ablate successive planes at a depth of 10 μm each. Samples were stained with 5-hexadecanoylamino-fluorescein and imaged with two-photon microscopy. Adapted from Tsai *et al*. [39].

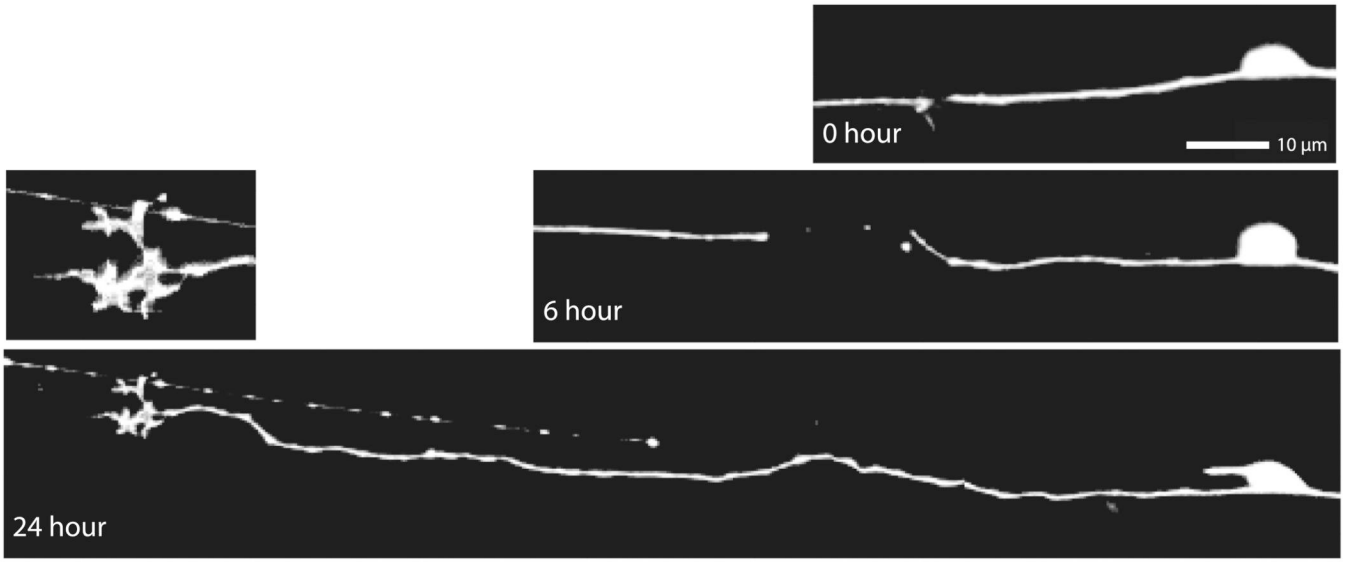

Figure 3. Time course of a regenerating touch neuron after plasma-assisted ablation

A mechanosensory PLM axon of *C. elegans* was severed (0 hour image). Following a quiescent phase (6 hour image), a growth cone appeared at the severed end and axon elongated in an imprecise manner (24 hour image). Adapted from Wu *et al*. [49].

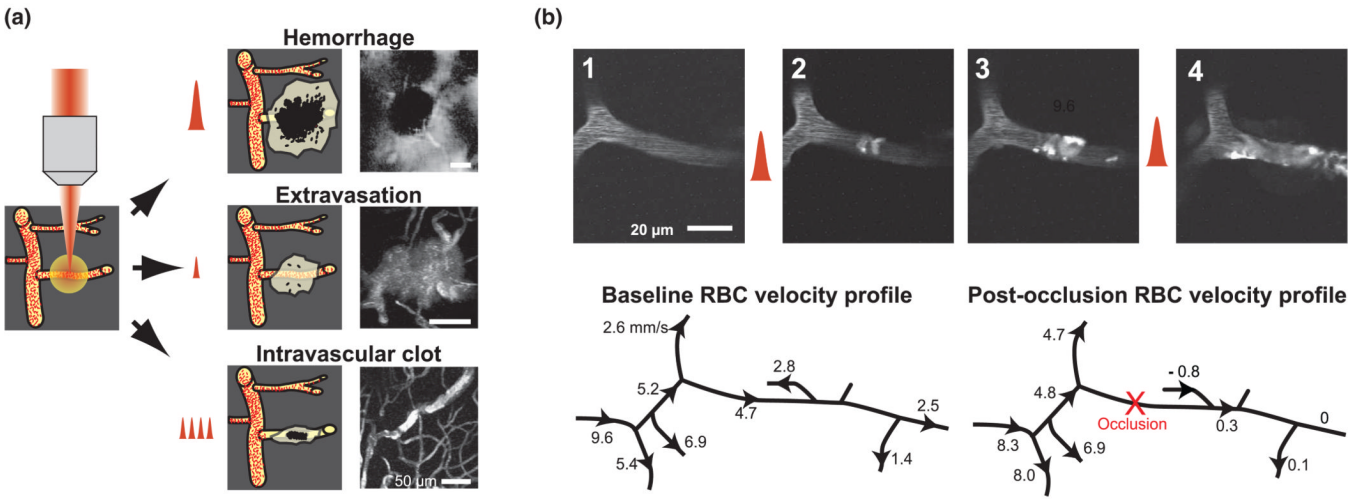

Figure 4. Application of plasma-mediated ablation to neurovascular studies

(a) Schematic of the three different lessions to subsurface neocortical vasculature that are produced by varying the energy and number of laser pulses. At high energies, photodisruption produces hemorrhages, in which the target vessel is ruptured, blood invades the brain tissue, and a mass of red blood cells (RBCs) form a hemorrhagic core. At low energies, but still above the threshold for plasma formation, the target vessel remains intact, but transiently leaks blood plasma and RBCs forming an extravasation. Multiple pulses at low energy led to thrombosis that can completely occlude the target vessel, forming an intravascular clot. (*b*) Formation of intravascular occlusions in deep microvessels using amplified hundred-femtosecond laser pulses. Images 1 to 4 are planar images taken from a region of interest with two-photo microscopy that depict the time-course for intravascular clot formation in a specific, 10 µm diameter vessel that lies ~ 200 µm below the surface. The red pulses indicate irradiation with multiple trains of 0.03 µJ pulses delivered at 1 kHz. The vascular traces show baseline and post-occlusion RBC velocity profiles, in mm/s, of the vascular network. Arrow-heads denote the direction of RBC movement and the red cross marks the occluded microvessel. Adapted from Nishimura *et al*. [40] and Helmchen and Kleinfeld [71].

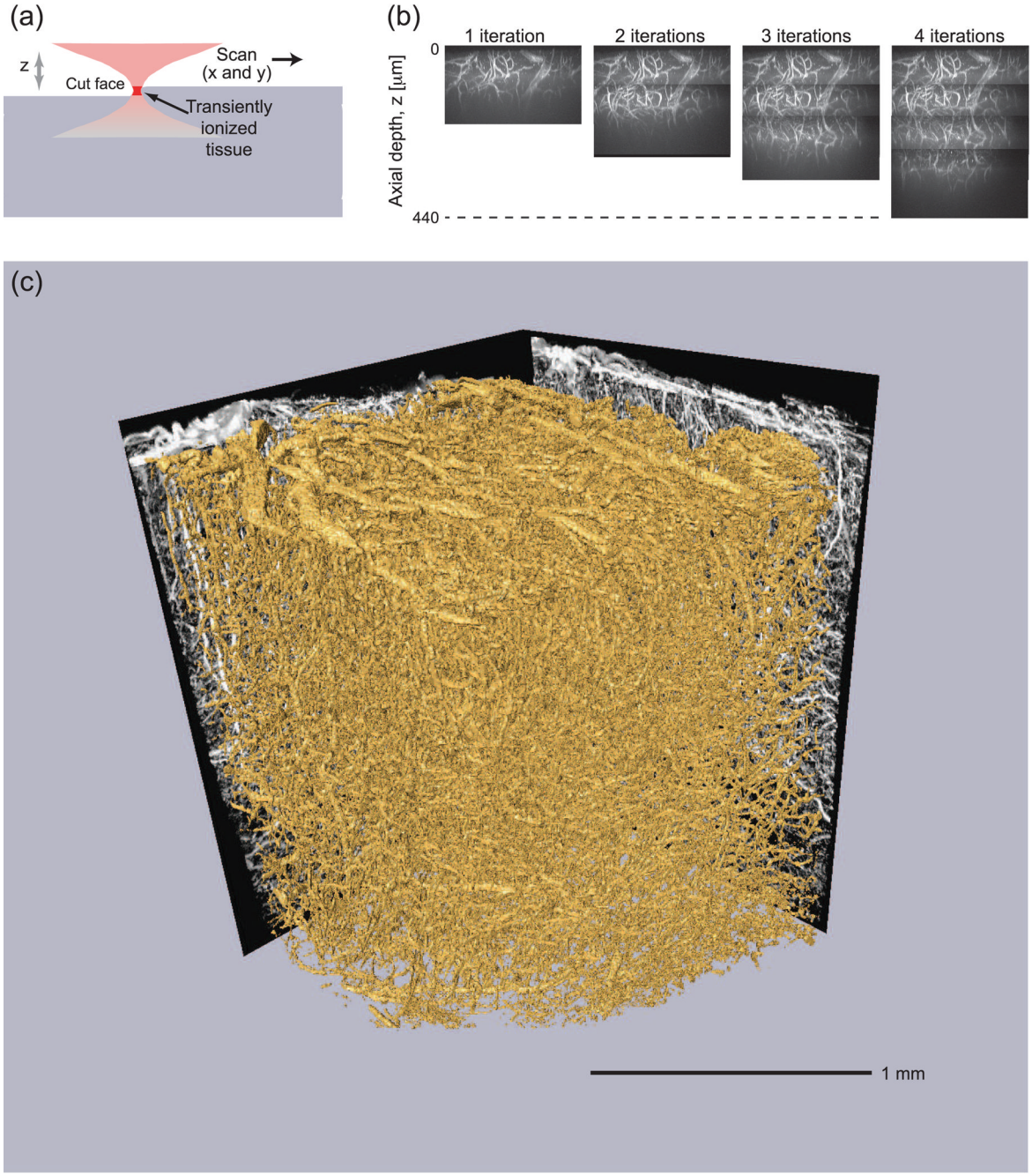

Figure 5. Plasma-mediated ablation, two-photon optical sectioning, and volumetric reconstruction for all optical histology of labeled vasculature in mouse neocortical tissue

(a) Schematic of the ablation process. The focus region is in red; this region approximately corresponds to the 10 to 100 fL ablation volume at the threshold energy for plasma formation. Adapted from Tsai *et al*. [39]. **(b)** Serial reconstruction of vasculature in a block of neocortex of a transgenic mouse in which actin filaments in the vascular wall is endogenously labeled with cyan fluorescent protein labeled. Four successive cutting and imaging cycles are shown. The laser was focused onto the cut face with a intermediate numerical aperture (0.5 NA) objective and a raster patterns of single passes were made to optically ablate successive planes at a depth of 10 μm each with total thicknesses of 70 μm

per cut. The energy per pulse varied from 0.4 to 1.7 μJ. Each stack of images represents a maximal side projection of all accumulated optical sections. The sharp breaks in the images shown in successive panels demarcate the cut boundaries. Adapted from Tsai *et al*. [39]. **(c)** Large volume (1.5 mm^3) reconstruction of block-face data obtained from mouse neocortex. The vasculature was filled with fluorescein-labeled agarose. Ablation of was performed by rastering the beam, with pulse energies of 5 μJ, as in part b. The image data consisted on overlapping stacks, 256 μm × 256 μm × 160 μm, that were registered into a single volume by means of cross-correlation over nearest neighbor features in the overlap region.

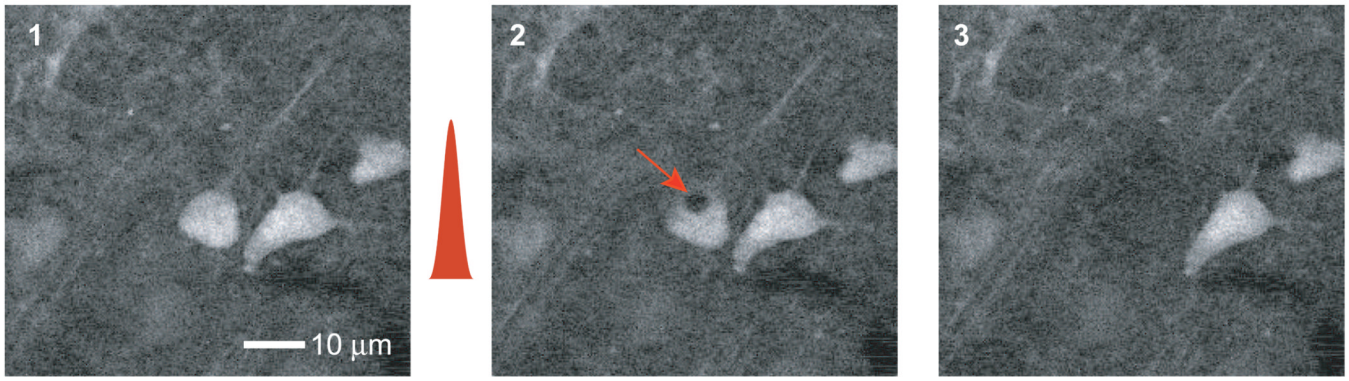

Figure 6. Application of plasma-mediated ablation to single-neuron studies in brain slice

A coronal brain slice from a P18 mouse in which pyramidal neurons are endogenously labeled with yellow fluorescent protein was imaged with two photon microscopy. All images are at a depth of 50 µm. The first image was obtained prior to laser ablation. The second image was taken within 1 s of single 0.04 µJ pulse to the targeted neuron (red arrow) with a high numerical (0.9 NA) objective. A bubble results from the ablation and collapses after ~ 2 s. The target neuron then slowly fades. By the third image, taken 160 s after the ablation pulse, the target cell is no longer visible as the endogenous cytosolic fluorescence has leaked. Note that neighboring pyramidal neurons remain sharply in focus and maintain their fluorescence and morphology.